ADVANCES IN ATMOSPHERIC SCIENCES, VOL. 24, NO. 1, 2007, 44–54

Potential Vorticity Structure and Inversion of the Cyclogenesis Over the Yangtze River and Huaihe River Valleys

ZHAO Bingke*[1,2] (赵兵科), WU Guoxiong[2] (吴国雄), and YAO Xiuping[2,3] (姚秀萍)

[1] *Shanghai Typhoon Institute, China Meteorological Administration, Shanghai* 200030

[2] *Institute of Atmospheric Physics, Chinese Academy of Sciences, Beijing* 100029

[3] *China Meteorological Administration Training Center, Beijing* 100081

(Received 16 September 2005; revised 13 April 2006)

ABSTRACT

In this paper, the potential vorticity structure and inversion of the cyclogenesis over the Yangtze River and Huaihe River valleys during 21–23 June 2003 are investigated with a potential vorticity (PV) framework. The cyclogenesis is manifested by a lower-tropospheric PV anomaly over the Yangtze River and Huaihe River valleys at early stages mainly due to latent heat release, which greatly affects the evolution of the associated lower-tropospheric geopotential height and wind fields as demonstrated by piecewise PV inversion. At later stages, an upper-tropospheric PV anomaly develops, resulting in the growth of ridges over the cyclone in both the upstream and downstream, which provide a favorable background field for the low-level cyclone development. But the effect of a surface thermal anomaly always impedes the development of the cyclone to different extents during this cyclogenesis. It is further demonstrated that the position and the strength of the PV anomaly are closely related to the low-level cyclone development, and the lower-tropospheric PV anomaly seems to constitute the most significant feature, for instance, contributing about 60% to the low-level jet (LLJ).

Key words: potential vorticity anomaly, potential vorticity inversion, latent heat release, low-level jet, cyclogenesis

DOI: 10.1007/s00376-007-0044-7

1. Introduction

Torrential rain is a major meteorological threat in the Yangtze River and Huaihe River valleys, especially during the late spring and summer. The resulting heavy flash floods are relatively common and disastrous events causing losses of human life and property are documented almost every year. Following the summers of 1991 and 1998, severe flooding occurred again in the Yangtze River and Huaihe River valleys in the summer of 2003, resulting from torrential rains induced by the continuous development of meso-scale cyclones or small low vortex systems.

The cyclogenesis over the Yangtze River and Huaihe River valleys has long been studied. In one case, a study based on the Ertel PV diagnosis, Hou (1991) pointed out that a mid-level, weak disturbance that originates from around the Qinghai-Tibetan Plateau may cause heavy rainfall under favorable conditions, and latent heat release in the mid-troposphere may lead to cyclonic circulation extending below the cyclonic circulation. Xing and Zheng (1999) demonstrated that the asymmetric structure of a meso-scale cyclone plays an important role in the development of a cyclone in their simulation of a heavy rainfall over the Yangtze River and Huaihe River valleys. Ma et al. (2002) indicated that the enhancement of the vertical shear of wind and the development of the upper jet stream are favorable to the initial cyclone development over the East China Sea. By simulating the development of Changjiang-Huaihe cyclones by a mesoscale numerical model, Li et al. (2002) suggested that besides the uplifting effect, the Dabie Mountain can induce differential temperature advection across Changjiang-Huaihe cyclones and increase the atmospheric instability. Using the PV inversion method, comparisons among the upper-, middle-, and low-level tropospheric PV perturbations, as well as their effects

*E-mail: zhaobk@mail.typhoon.gov.cn

on the initiation of an MCS, Peng et al. (2002) indicated that the low-level tropospheric PV perturbations play an important role in the triggering of an MCS. Chen et al. (2003) used PV diagnostic skill and found the positive feedback between the Mei-yu frontogenesis and cumulus latent heating, in which the front provides low-level convergence and helps organize the convection while latent heating by cumuli generates low-level PV and further enhances the frontogenetic process, leading to rapid growth in shear vorticity along the front. Tao et al. (2004) showed that the vertical motion induced by a positive vorticity advection in the front of the upper trough and a warm advection in the low levels urge the development of a surface cyclone. Zhao et al. (2004) revealed that the positive vorticity, from a low level convergence, is the direct dynamic factor in the development of a cyclone. However, the role of dynamic forcing conditions at the different levels on the low level cyclogenesis over the Yangtze River and Huaihe River valleys has not yet been investigated in depth. Much work remains to be done in order to increase our understanding on the dynamics of cyclogenesis.

Because of the conservation property and invertibility of PV (Hoskins et al., 1985), the PV concept and inversion techniques have been widely applied by researchers in recent years. Different methods of PV inversion have been used for individual cases of cyclogenesis by Robinsion (1988), Davis and Emanuel (1991, hereafter DE), Black and Dole (1993), and Parker and Thorpe (1995). The nonlinear balanced piecewise PV inversion technique developed by DE has been chosen as our primary tool of diagnosis, mainly because it allows partitioning among different processes, thereby isolating of their individual contributions.

The current study presents an analysis of an intense case of cyclogenesis that occurred over the Yangtze River and Huaihe River valleys during 21-23 June 2003, accompanied by a strong LLJ (the southerly is over 12 m s^{-1} at 850 hPa) and a torrential rain process. The objective of this study is to investigate the dynamics of this case with the PV framework, and to primarily study and assess the individual contributions of the key dynamic features at the different levels to the wind field by using piecewise PV inversion. Section 2 describes the data and the methodology. Section 3 provides a synoptic overview, followed by a presentation of the PV inversion in section 4. Section 5 contains a summary and discussion.

2. Data and methodology

The data used in this study are from the China Meteorological Administration (CMA), including 6-hourly precipitation at 730 weather observation stations. Six-hourly (at 0000, 0600, 1200, and 1800 UTC) gridded operational analyses from the National Centers for Environmental Prediction (NCEP) are adopted as our primary data for calculation and diagnosis. Two datasets, with 1.0° × 1.0° and 2.5° × 2.5° latitude-longitude grids, include geopotential height, temperature, u and v components of horizontal wind, vertical velocity ω, and relative humidity at twenty-one pressure levels (1000, 975, 950, 925, 900, 850, 800, 750, 700, 650, 600, 550, 500, 450, 400, 350, 300, 250, 200, 150, and 100 hPa). The latter is only used for the PV inversion.

In this study, we use the technique of nonlinear balanced PV inversion, which is described in detail in the literature (DE; Davis, 1992a, b). Here, it is described briefly. Based upon the Charney nonlinear balance (Charney, 1955), DE's scheme assumes (1) hydrostatic balance and (2) that the magnitude of the irrotational component of the wind is much smaller than the magnitude of the nondivergent component. Applying these approximations to the divergence equation and definition of Ertel PV (EPV) results in the invertibility relationship for this system (transformed to spherical coordinates):

$$\nabla^2\Phi = \nabla\cdot f\nabla\Psi + \frac{2}{a^4\cos^2\phi}\left[\frac{\partial^2\Psi}{\partial\lambda^2}\frac{\partial^2\Psi}{\partial\phi^2} - \left(\frac{\partial^2\Psi}{\partial\lambda\partial\phi}\right)^2\right], \quad (1)$$

$$\mathrm{EPV} = \frac{gk\pi}{p}\left[(f+\nabla^2\Psi)\frac{\partial^2\Phi}{\partial\pi^2} - \frac{1}{a^2\cos^2\phi}\frac{\partial^2\Psi}{\partial\lambda\partial\pi}\frac{\partial^2\Phi}{\partial\lambda\partial\pi} - \frac{1}{a^2}\frac{\partial^2\Psi}{\partial\phi\partial\pi}\frac{\partial^2\Phi}{\partial\phi\partial\pi}\right], \quad (2)$$

where $\Phi, \Psi, \lambda, \phi, f, a, g, p$, and EPV are, respectively, geopotential, streamfunction for the nondivergent wind, longitude, latitude, Coriolis parameter, earth's radius, gravitational acceleration, pressure, and potential vorticity; $k = R/c_p$, and π is the Exner function $[c_p(p/p_0)^k]$, which serves as the vertical coordinate.

Given a known distribution of Ertel PV and specified boundary conditions, Φ and Ψ can be solved. Here, we adopt Neumann boundary conditions as the top and bottom boundaries and Dirichlet ones as the lateral boundaries. First, the aforementioned relations (1) and (2) are nondimensionalized and written in the form of difference equations. Thus, a set of equations is obtained. If the static stability and absolute vorticity are positive, they are elliptic equations and simple two-dimensional Poisson equations. Then, by the iteration method, we can get solutions of Ψ and Φ. Here,

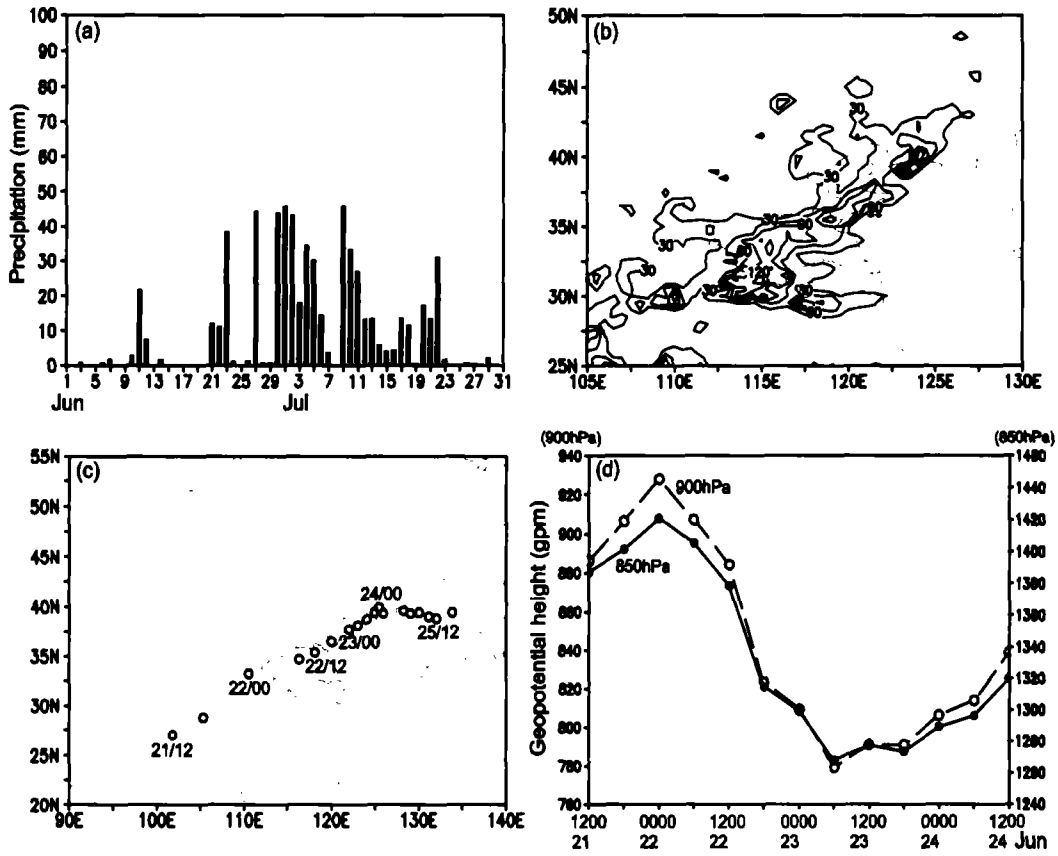

Fig. 1. (a) The evolution of averaged daily precipitation of the Huaihe River valley (31.5°–34.5°N, 115°–120°E) during June and July 2003. (b) Distribution of accumulative precipitation from 0000 UTC 21 to 0000 UTC 24 June 2003 with a contour interval of 30 mm. (c) The path of the cyclone at 850 hPa, where circles mark the locations of the cyclone center. (d) Intensitiy evolution of the 850 and 900 hPa geopotential heights at the cyclone center; y-coordinate is for the geopotential height (gpm).

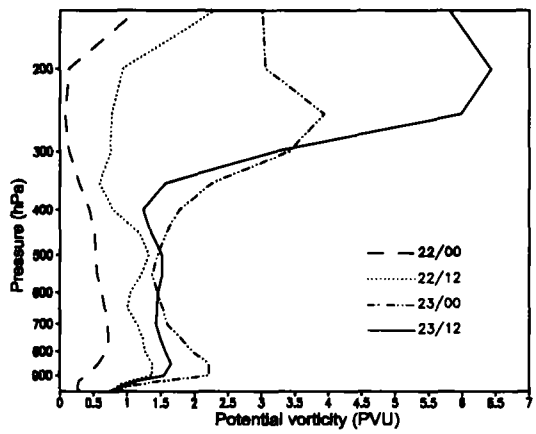

Fig. 2. Vertical distribution of the nine-point-averaged PV (PVU) of the cyclone center at 850 hPa.

standard successive overrelaxation (SOR) is adopted. In addition, the ellipticity of the equations to be solved is dependent on the PV being positive. Negative values of observed PV are set to a small positive constant (10^{-2} PVU, potential vorticity units, 1PVU=1.0×10^{-6} m^2 s^{-1} K kg^{-1}). Finally, the zonal wind U and meridional wind V are obtained from the Ψ by:

$$U = -\frac{\partial \Psi}{\partial y}, \quad V = \frac{\partial \Psi}{\partial x}.$$

Of course, other elements, such as air temperature T and relative vorticity VOR, etc., can also be obtained from Φ and Ψ.

DE demonstrated that the Charney nonlinear balance equation is an excellent approximation to observed flows, thus validating the application of PV diagnostics to the real atmosphere.

Following DE, to achieve piecewise PV inversion, the mean and perturbation fields must be first defined. Researchers often choose the life span average of a weather system as the mean field (e.g., Davis, 1992a; Bresky and Colucci, 1996; Chen et al., 2003; Martin and Marsili, 2002; Martin and Otkin, 2004). We adopt

a time average of 21–26 June 2003 as the mean field. In order to eliminate the diurnal variation, the mean field and the PV inversion are calculated four times a day (at 0000, 0600, 1200, and 1800 UTC). The difference between an instantaneous PV field and the corresponding mean PV field is referred to as the perturbation PV field for that time. A conventional three-way partitioning of the total perturbation PV field into an upper layer, an interior layer, and a surface layer in the present study follows that of DE, but it is modified slightly to fit the outline of our case. The upper layer component, which is designed to isolate PV anomalies associated with undulations in the upper troposphere, includes PV perturbations from 500 to 150 hPa and the potential temperature perturbation at 125 hPa. The interior layer component includes PV perturbations from 950 to 550 hPa and is designed to isolate lower-tropospheric PV anomalies associated with latent heat release. Latent heat release occurs only in environments at or near saturation where the relative humidity is greater than or equal to 70%. Finally, the surface layer, designed to isolate the boundary potential temperature anomalies that are equivalent to PV anomalies just above the surface (Bretherton, 1966), includes the 975-hPa potential temperature perturbations. For the remainder of the paper, UP refers to perturbations associated with the upper layer, IP to perturbations associated with the interior layer, and SP to perturbations associated with the surface layer.

3. Synoptic overview

3.1 *Low-level cyclone evolution*

From 21 June to 22 July 2003, heavy precipitation processes occurred frequently over the Huaihe River valley. There are six torrential rain processes during the period, occurring on 21–23 June, 27 June, 30 June–6 July, 9–14 July, 17–18 July, and 20–22 July (Fig. 1a). The detailed descriptions of these may be seen from Zhao et al. (2005). The occurrence of each torrential rain is always accompanied by a cyclogenesis and a cyclolysis. Meanwhile, each system is also accompanied by widespread heavy rainfall that results in flooding in the Huaihe River valley. Here, we select the first torrential rain process, 21–23 June, as our study object. The distribution of precipitation for this process can be seen in Fig. 1b. Figure 1c presents an evolution of the path of the cyclone at 850 hPa. At first, at 1200 UTC 21 June (from this point forward, the date and time will be referenced as Day/Hour, e.g. 21/12 is 1200 UTC 21 June), the cyclone is located at the southwest of Sichuan province, then, it moves northeastwards. At 22/00, it is close to the Huaihe River valley. Between 22/00 and 22/18, it is over the Huaihe River valley. Continuing northeastwards, it is located over the northern Huanghai Sea from 23/00 through 24/00. After 24/00, it moves eastwards. At 24/12, it reaches over the southern part of the Japan Sea. Continuing to move eastwards, after 26/18, it disappears over the Northwest Pacific Ocean. The intensity evolutions of the 850 and 900 hPa geopotential heights at the cyclone center are displayed in Fig. 1d. Their tendencies are very similar. The cyclones develop continuously from 22/00 to 23/06, particularly showing a rapid development between 22/12 and 22/18. After 23/06, they weaken gradually.

3.2 *Development of the cyclone from the Lagrangian standpoint*

To describe the development of the cyclone, we track it from the Lagrangian viewpoint. Figure 2 shows the vertical distribution of the nine-point-averaged PV of the 850-hPa cyclone center for the period from 22/00 through 23/12. At 22/00, a relatively small PV at the cyclone center is observed throughout the troposphere, and its maximum, only 0.7 PVU, is located near 800 hPa. After 12h, at 22/12, the PV maximum at 850 hPa has strengthened to about 1.5 PVU. By 22/18, only 6 h later, the PV at low levels rises evidently when the PV at upper levels is augmented, from 1 to 2.5 PVU. Subsequently, the intensification of the PV mainly shows at upper levels.

In short, the cyclone at first develops at low levels, then it starts to expand rapidly once the upper level system moves over the cyclone at low levels and intensifies markedly.

3.3 *Potential vorticity features in the mid-upper troposphere*

Figure 3 presents the evolution of the PV and Montgomery streamfunction fields on the 340 K isentropic surface from 22/00 to 23/12. It stands for the activity characteristics of the upper-tropospheric circulation. An important feature is a PV streamer that extends southeastwards and wraps around, which associated closely with the cyclogenesis. At 22/00, the front part of the PV streamer is located over the central part of Shaanxi Province, coinciding with the upper level trough (Fig. 3a). It develops toward the southeast. By 22/12, it reaches over the north of the Huaihe River valley and intensifies clearly (Fig. 3b). From Fig. 3c, it can be seen that in the subsequent twelve hours, the PV streamer becomes more zonally oriented at its southern edge. At 23/12, the PV streamer wraps around and a maximum value of 7 PVU is located over the north of the Huaihe River valley (Fig. 3d). In addition, it can be seen that the cyclone at the low levels, at first, is centered to the so-

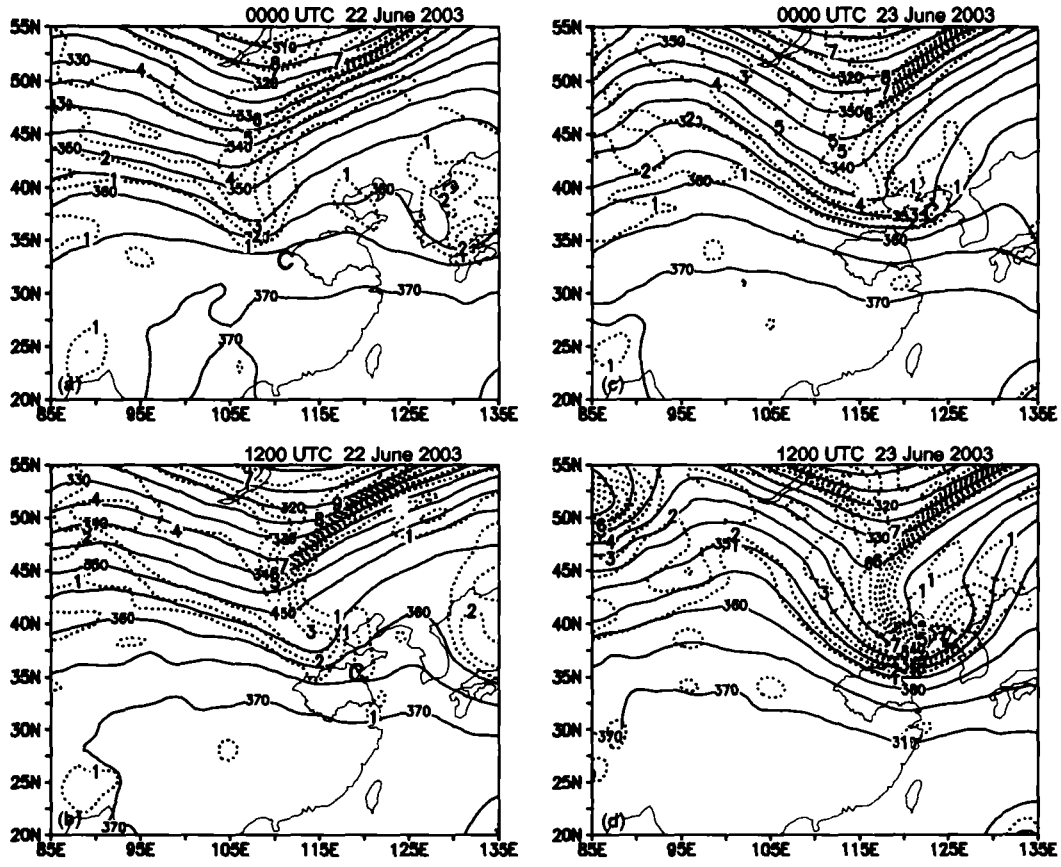

Fig. 3. Isentropic analyses at 340 K of the Montgomery streamfunction (solid, 340=3.340×10^5 m^2 s^{-2}) and PV (dotted, PVU) at (a) 0000 UTC 22 June 2003; (b) 1200 UTC 22 June 2003; (c) 0000 UTC 23 June 2003; (d) 1200 UTC 23 June 2003. C is the location of the 850 hPa cyclone center.

utheast of the PV streamer, and in the end, it is located below the north of the PV streamer.

The evolutions of the PV and Montgomery streamfunction fields on the 320 K isentropic surface from 22/00 to 23/12 are shown in Fig. 4. They can be regarded as the activity characteristics of the atmosphere at mid-tropospheric levels. They mainly reflect an obvious enhancing process of the extratropical frontal zone. At 22/00, the extratropical frontal zone is weak and deviates from the polar frontal zone as observed from the PV distribution. An area of PV greater than 1 PVU is located over the northwest of the Huaihe River valley (Fig. 4a). By 22/12, one can see a clear supplement of PV from the polar frontal zone into the extratropical frontal zone. The area of PV greater than 1 PVU is enlarged remarkably and moves eastwards (Fig. 4b). By 23/00, the extratropical frontal zone greatly intensifies, and the PV maximum over Bohai also strengthens to over 1.5 PVU (Fig. 4c). One can see a strong extratropical frontal zone and an evident ridge upstream by 23/12 (Fig. 4d).

3.4 *Vertical structure of potential vorticity*

In order to examine the vertical structure of PV anomalies involved in the cyclone development, Fig. 5 displays longitude-height cross sections of meridional wind, PV, and potential temperature across the 850 hPa cyclone center. It can be seen that the upper- and lower-level PV anomalies intensify evidently, the LLJ on the east of the lower-level PV anomaly is amplified clearly, and the baroclinity over the cyclone is augmented remarkably during the cyclone development. At 22/00, the low-level cyclone is located over the west of the Huaihe River valley while the mid-lower troposphere PV maximum, with a 900–400 hPa layer-average PV in excess of 0.75 PVU, is immediately to the east of it. To the east of this PV maximum, a southerly, with 950–600 hPa layer-average wind speeds in excess of 10 m s^{-1}, is over the Huaihe River valley. In addition, to the west of this cyclone center, there is

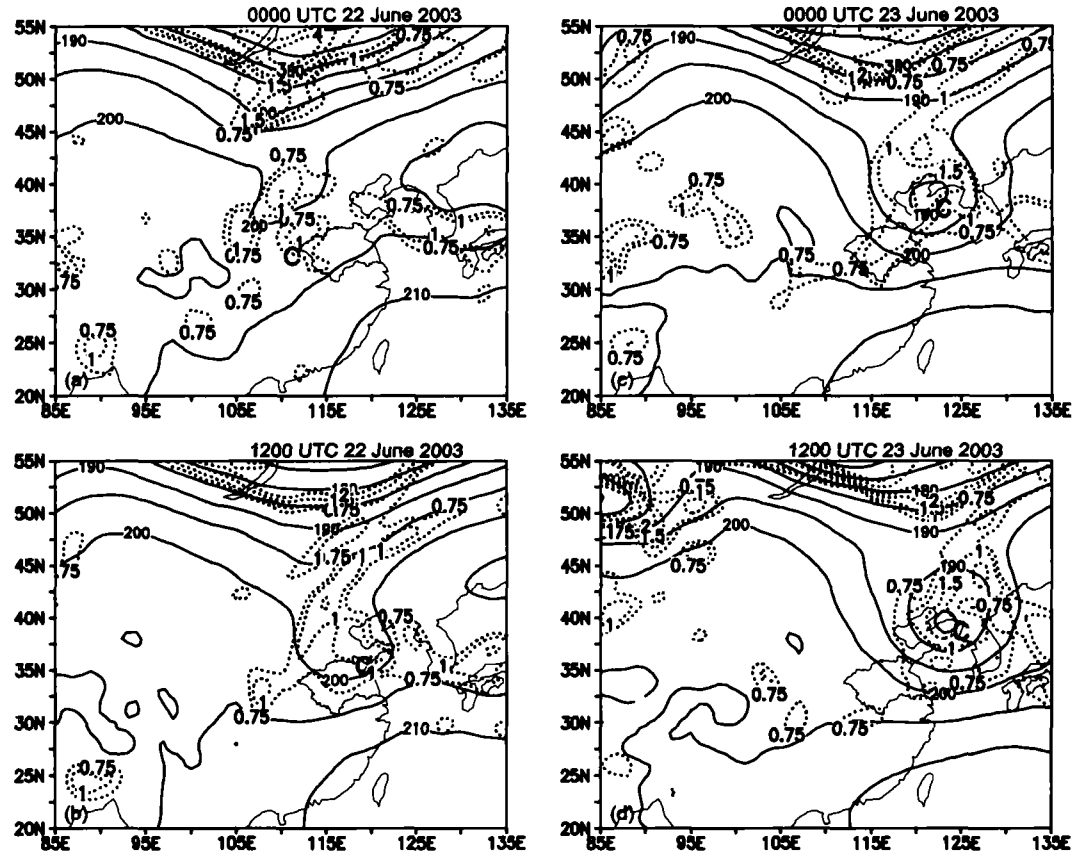

Fig. 4. Isentropic analyses at 320 K of the Montgomery streamfunction (solid, 200=3.200×10^5 m^2 s^{-2}) and PV (dotted, PVU) at (a) 0000 UTC 22 June 2003; (b) 1200 UTC 22 June 2003; (c) 0000 UTC 23 June 2003; (d) 1200 UTC 23 June 2003. C is the location of the 850 hPa cyclone center.

another PV maximum. A northerly with wind speeds in excess of 10 m s^{-1} is located on its western side. The isotropic lines are almost level (Fig. 5a). By 22/12, the cyclone reaches over the north of the Huaihe River valley and is intensified clearly, with the PV maximum over 1.5 PVU at around 850 hPa. The southerly to the east of it is intensified by 10 m s^{-1} between 22/00 and 22/12. An upper-tropospheric PV anomaly to the west of it extends downwards and is accompanied by a southerly with wind speeds of 5 m s^{-1} on its eastern side. The isotropic lines in the vicinity of the cyclone center are slight tilted (Fig. 5b). By 23/00, the cyclone reaches over the northern Huanghai Sea. The PV maximum at around 850 hPa is over 2.5 PVU and a strong upper PV anomaly of more than 5 PVU extends downwards. Thus, it can be seen that an upstanding PV post is in the cyclone center from the lower to upper troposphere. The low-level cyclone reaches its peak intensity when both the upper- and low-tropospheric maximum positive PV anomalies overlap over the lower-level cyclone without vertical tilting. A vertical southerly column, with wind speeds in excess of 20 m s^{-1}, is on its eastern side. The isotropic lines lean remarkably in the vicinity of the cyclone center (Fig. 5c). By 23/12, the cyclone starts to weaken. In addition, for the surface thermal field, a "tilt" in isotropic lines is noticed in the vicinity of the cyclone center. From Fig. 5b and c, one can see that near the surface there are two cold anomalies and one warm anomaly between them, with the cyclone center located between the western cold and the warm anomalies.

4. Potential vorticity inversion

The aforementioned analyses demonstrate that the cyclogenesis is featured by strong upper- and low-level PV anomalies. Of course, we should also pay attention to the surface thermal anomaly. In order to determine quantitatively the dynamical contribution of each of

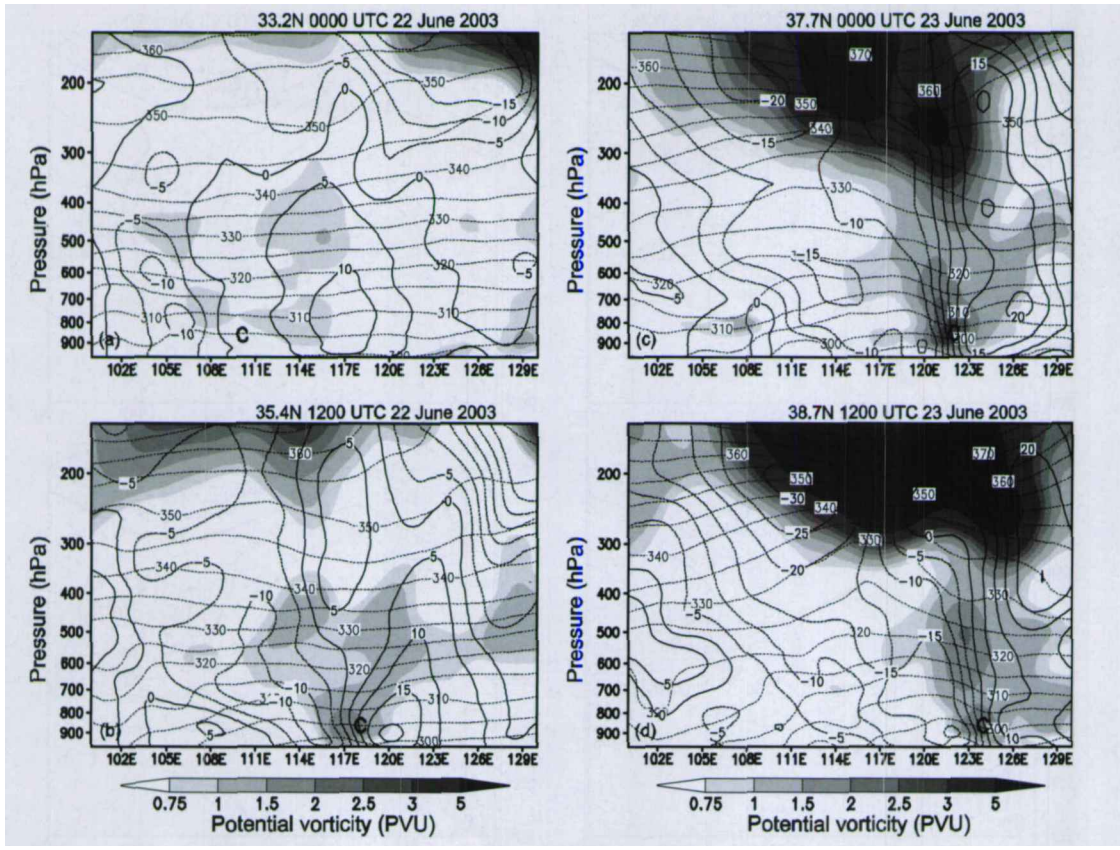

Fig. 5. Longitude-height cross sections of meridional wind (thick line, m s^{-1}), PV (shaded, PVU), and potential temperature (thin dashed, K) along the cyclone center at 850 hPa for (a) 0000 UTC 22 June 2003; (b) 1200 UTC 22 June 2003; (c) 0000 UTC 23 June 2003; (d) 1200 UTC 23 June 2003. C is the location of the 850 hPa cyclone center.

these features to the low-level cyclone development, piecewise PV inversions are performed.

Figure 6 shows cross sections of contributions to the total perturbation geopotential height induced by the upper- and lower-tropospheric PV disturbances as well as the surface thermal anomaly for 22/12 (left column) and 23/00 (right column). At 22/12, the geopotential height field associated with the upper PV exhibits positive anomalies in the upper-tropospheric upstream and particularly in the downstream regions over the cyclone. By 23/00, the positive anomalies clearly intensify and extend downwards. However, the geopotential height field is inverted from the lower PV; at 22/12, it not only shows positive anomalies in the low-tropospheric upstream and downstream regions over the cyclone but also displays a negative anomaly in the cyclone area. By 23/00, the negative anomaly evidently strengthens and the positive anomalies disappear. The geopotential height anomaly induced by the surface thermal anomaly is just opposite to that induced by the lower PV.

To illustrate the relationship between the LLJ* and PV anomalies, Fig. 7 displays cross sections of contributions to the total perturbation meridional wind associated with the upper- and lower-tropospheric PV disturbances as well as the surface thermal anomaly. It can be seen that the southerly associated with the upper PV anomaly is on its eastern side and a northerly is on its western side. Before the cyclone reaches its maximum intensity, they clearly extend downwards. The distribution of the wind field induced by the lower PV anomaly is equiform with that by the upper, namely the southerly on its eastern side and the northerly on its western side. An opposite wind field associated with the surface thermal anomaly is in the lower-level. It can be seen that the center of the low-level cyclone is located in the area of the southerlies induced by the upper- and lower-tropospheric PV anomalies, but located in the area of the northerly induced by the surface thermal anomaly. The northerly has a clear intensification when the low-level cyclone reaches its peak intensity. In addition, the upper- and lower-tropospheric PV anomalies are found to account for about 20% and 60%, respectively, of the total inverted

*Here LLJ only implies its perturbation part.

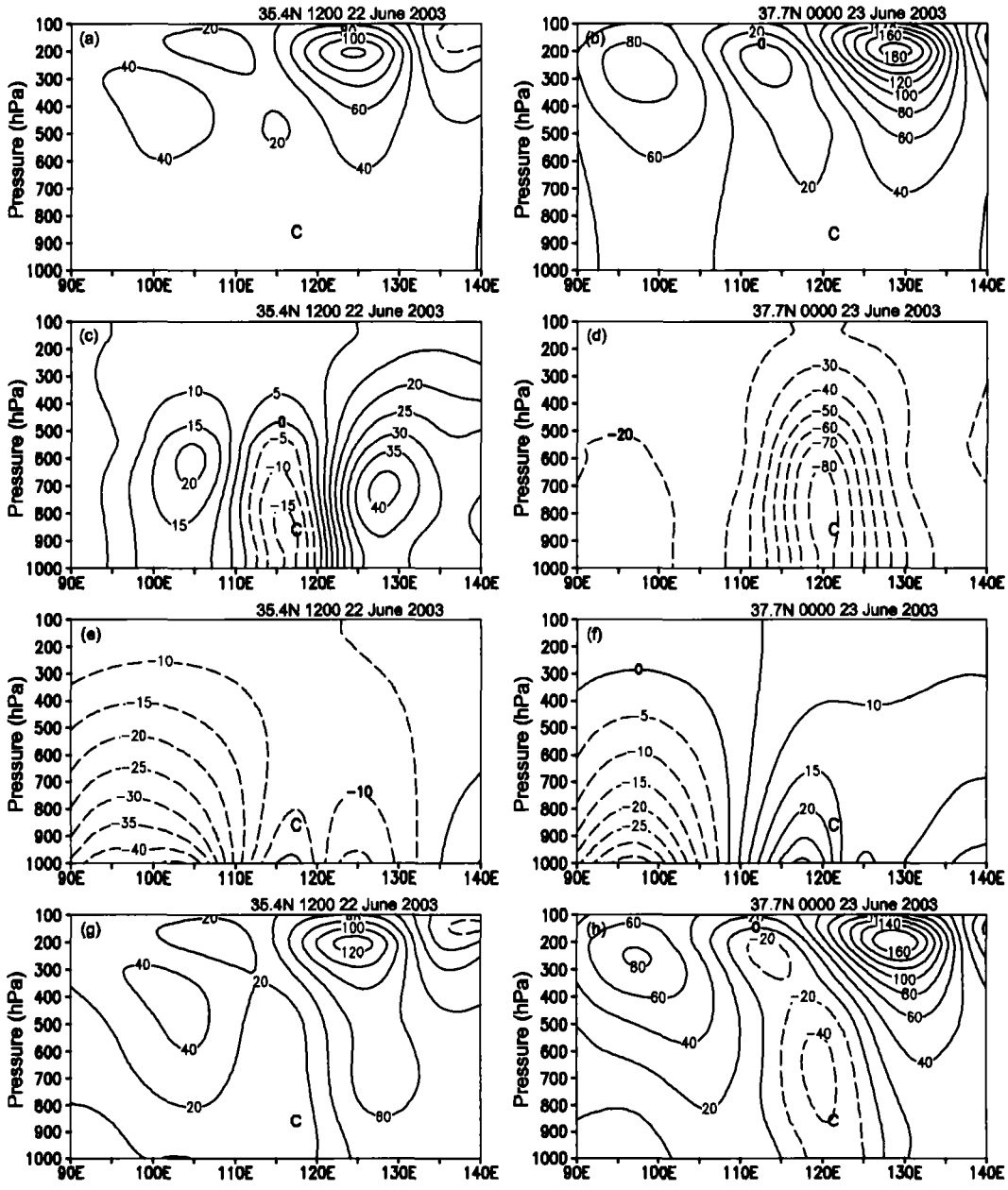

Fig. 6. Longitude-height cross sections of geopotential height perturbations. Left column is for 1200 UTC 22 June 2003, right column is for 0000 UTC 23 June 2003. Panels (a) and (b) show height perturbations associated with the UP; (c) and (d) from IP; (e) and (f) from SP; (g) and (h) are total balanced height perturbations (unit: gpm). C is the location of the 850 hPa cyclone center.

southerly at the lower level. This implies that the lower-tropospheric PV plays an important role in the evolution of the low-level cyclone.

Furthermore, by analyzing the relations between the aspects of the PV anomaly and the evolution of the low-level cyclone, we can see that the position and strength of the PV anomaly are closely related to the low-level cyclone development. In fact, the intensity of the cyclone is also expressed by its PV anomaly, namely the stronger PV anomaly becomes, the more the cyclone gets. This has been validated by a few ideal tests of PV inversion (Zhao, 2006). The importance of the lower-tropospheric PV can also be seen in Fig. 8, which shows the time series of averaged relative vorticity of the cyclone center at 850 hPa, partitioning the contributions from different processes (UP, IP, and

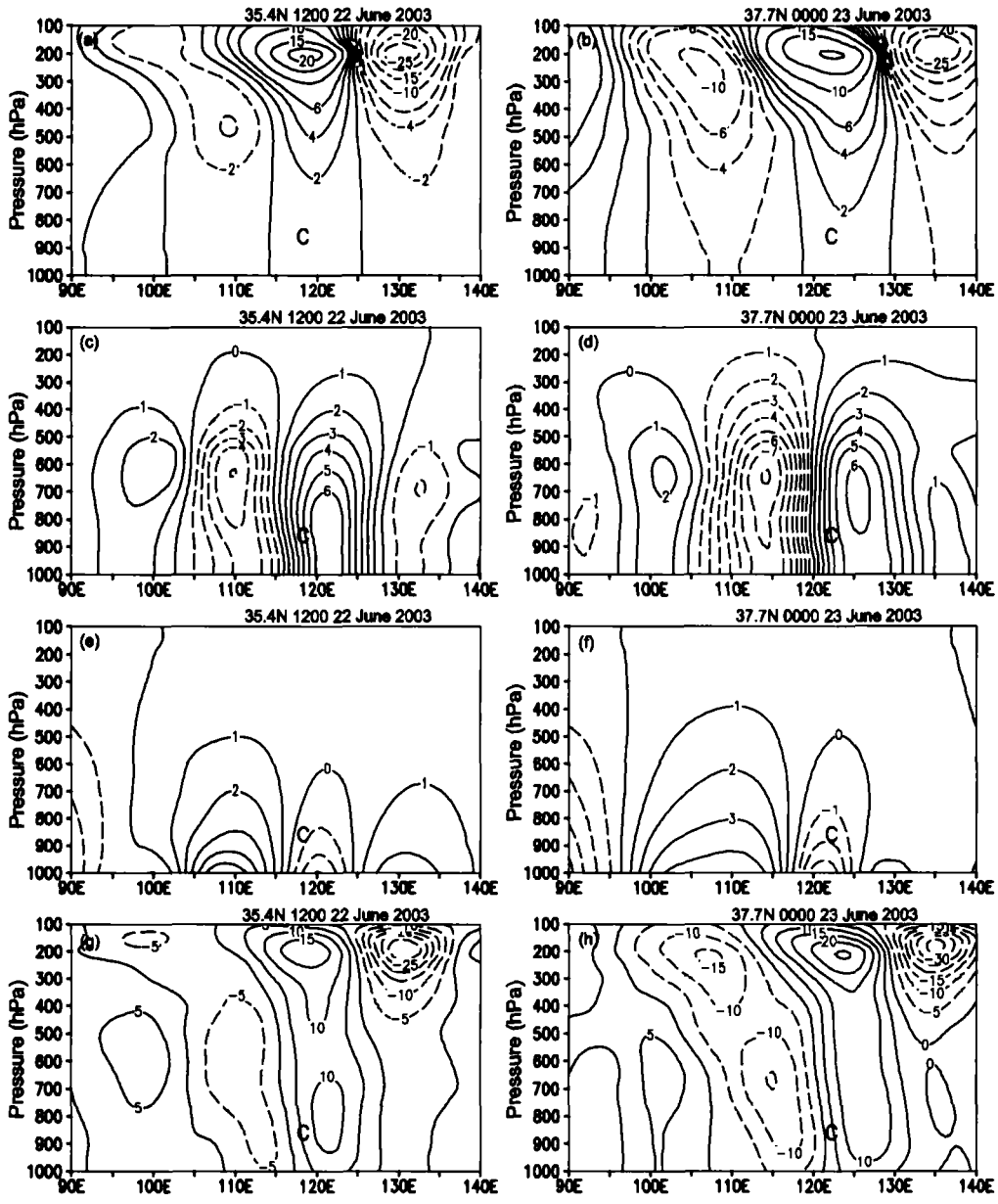

Fig. 7. As in Fig. 6 except for meridional wind (unit: m s^{-1}).

SP) towards total vorticity. Very clearly, at early stages, the low-level vorticity is responsible for its significant direct contribution to the low-level cyclone. At later stages, the upper-tropospheric vorticity has a rapid intensification. The surface thermal anomaly always shows a negative contribution during the cyclone development.

5. Summary and discussion

The potential vorticity structure and inversion of the cyclogenesis over the Yangtze River and Huaihe River valleys during 21–23 June 2003 is investigated with the potential vorticity (PV) framework. Following a method developed by DE, we first identify a few distinct anomalies in the PV field. By successively inverting parts of the PV field, the quantitative contributions to the geopotential height and meridional wind fields are obtained from these anomalies. The major results can be summarized as the following:

At early stages, the cyclogenesis is manifested by a lower-tropospheric PV anomaly over the Yangtze River and Huaihe River valleys, mainly from latent heat release, which influences substantially the evolution of the low-tropospheric height and wind fields associated with the cyclone. At later stages, an upper-tropospheric PV anomaly development results in the growth of upstream and downstream positive anoma-

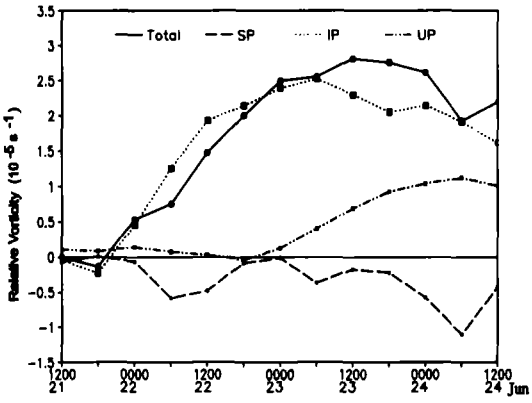

Fig. 8. Time series of the nine-point-averaged relative vorticity of the cyclone center at 850 hPa from the Lagrangian method. There is a partitioning of contributions from different processes (UP, IP, and SP) toward total vorticity. The abscissa indicates date and time, and the ordinate indicates relative vorticity (10^{-5} s^{-1}).

lies over the cyclone. It provides a favorable background field for the low-level cyclone development. But the effect of the surface thermal anomaly always blocks the development of the cyclone to a different extent during this cyclogenesis. By means of piecewise PV inversion, it is further demonstrated that the position and the strength of the PV anomaly are closely related to the low-level cyclone development, and the lower-tropospheric PV anomaly seems to constitute the most significant feature, for instance, contributing about 60% to low-level jet (LLJ).

Raymond (1992) showed that latent heating can enhance the cyclogenesis process in two ways. Firstly, saturated conditions can effectively reduce the static stability and enhance the vertical penetration of the circulation of the upper- and lower-boundary PV anomalies. Secondly, a maximum of diabatic heating produces a positive (negative) PV anomaly upshear (downshear) along the absolute vorticity vector. Previous studies have found that the impact of a lower tropospheric diabatically generated PV anomaly on cyclogenesis varies from case to case. In some cases, this anomaly is the primary contributor to the cyclogenesis (Reed et al., 1992) and can facilitate the phase locking and mutual amplification of the upper- and lower-boundary PV anomalies (Stoelinga, 1996). However, in other cases, the diabatic anomaly provides only a minor contribution to the cyclone strength, or it can actually inhibit phase-locking of the upper- and lower-boundary PV anomalies (Davis, 1992a). From the latent heat release, the example in our study, in which the lower-tropospheric PV anomaly, mainly from latent heat release, influences substantially the evolution of the low-tropospheric height and wind fields associated with the cyclone, is analogous to the one discussed by Reed et al. (1992). Exhilaratingly, Nielsen and Sass (2003) assessed the impact of latent release by performing numerical simulations with and without these heat sources in a severe storm over Denmark in December 1999. They demonstrated that the surface cyclone deepened to 978 hPa in the latter simulation as compared to 954 hPa in the simulation with latent heat release. Finally, they indicated that the release of latent heat played an important role in the cyclogenesis.

The remaining question is why the low-level PV was attributed solely to latent heating release. This will be answered by a PV budget analyses in a parallel study. It should be further examined why the surface thermal anomaly always blocks the development of the cyclone for this case. Further work is needed to investigate such extratropical cases with different intensities. Of course, the role of friction from the lower boundary should also be considered in future work.

Acknowledgements. The authors would like to thank Dr. Wang Zaizhi and Dr. Liu Yimin for their beneficial discussions. The authors thank the two reviewers for their constructive comments in improving the original manuscript. This work was also partly supported by the National Key Programme for Developing Basic Sciences (Grant No. 2004CB418300) and by the National Natural Sciences of China (NSFC) under Grant Nos. 40475027 and 40221503.

REFERENCES

Black, R. X., and R. M. Dole, 1993: The dynamics of a large-scale cyclogenesis over the North Pacific Ocean. *J. Atmos. Sci.*, **50**, 421–442.

Bresky, W. C., and S. J. Colucci, 1996: A forecast and analyzed cyclogenesis event diagnosed with potential vorticity. *Mon. Wea. Rev.*, **124**, 2227–2244.

Bretherton, F. P., 1966: Critical layer instability in baroclinic flows. *Quart. J. Roy. Meteor. Soc.*, **92**, 325–334.

Charney, J. G., 1955: The use of primitive equations of motion in numerical prediction. *Tellus*, **7**, 22–26.

Chen, G. T. J., C. C. Wang, and S. C. C. Liu, 2003: Potential vorticity diagnostics of a Mei-Yu front case. *Mon. Wea. Rev.*, **131**, 2680–2696.

Davis, C. A., 1992a: A potential-vorticity diagnosis of the importance of initial structure and condensational heating in observed extratropical cyclogenesis. *Mon. Wea. Rev.*, **120**, 2409–2428.

Davis, C. A., 1992b: Piecewise potential vorticity inversion. *J. Atmos. Sci.*, **49**, 1397–1411.

Davis, C. A., and K. A. Emanuel, 1991: Potential vorticity diagnostics of cyclogenesis. *Mon. Wea. Rev.*, **119**, 1929–1953.

Hoskins, B. J., M. E. McIntyre, and A.W. Robertson, 1985: On the use and significance of isentropic potential vorticity maps. *Quart. J. Roy. Meteor. Soc.*, **111**, 877–947.

Hou Dingchen, 1991: The potential vorticity structure of summer cyclones over the Changjiang-Huaihe valley. *Acta Meteorologica Sinica*, **49**, 141–150. (in Chinese)

Li Bai, Yu Weipin, Lu Yun, and Lu Dachun, 2002: The numerical simulation study of the mesoscale characteristics on the development of Jiang-Huai cyclones. *Scientia Meteorologica Sinica*, **22**, 72–80. (in Chinese)

Ma Leiming, Qin Zenghao, and Duan Yihong, 2002: Case study on the impact of atmospheric baroclinicity to the initial development of Jianghuai cyclones. *Acta Oceanologica Sinica*, **24**, 95–104.

Martin, J. E., and N. Marsili, 2002: Surface cyclolysis in the North Pacific Ocean. Part II: Piecewise potential vorticity diagnosis of a rapid cyclolysis event. *Mon. Wea. Rev.*, **130**, 1264–1281.

Martin, J. E., and J. A. Otkin, 2004: The rapid growth and decay of an extratropical cyclone over the central Pacific Ocean. *Wea. Forecasting*, **19**, 358–376.

Nielsen, N. W., and B. H. Sass, 2003: A numerical high-resolution study of the life cycle of the severe storm over Denmark on 3 December 1999. *Tellus*, 55A, 338–351.

Parker, D. J., and A. J. Thorpe, 1995: The role of snow sublimation in frontogenesis. *Quart. J. Roy. Meteor. Soc.*, **121**, 763–782.

Peng Jiayi, Wu Rongsheng, and Wang Yuan, 2002: Initiation mechanism of a meso-scale convective system. *Adv. Atmos. Sci.*, **19**, 870–884.

Raymond, D. J., 1992: Nonlinear balance and potential-vorticity thinking at large Rossby number. *Quart. J. Roy. Meteor. Soc.*, **118**, 987–1015.

Reed, R. J., M. T. Stoelinga, and Y.-H. Kuo, 1992: A model-aided study of the origin and evolution of the anomalously high potential vorticity in the inner region of a rapidly deepening marine cyclone. *Mon. Wea. Rev.*, **120**, 893–913.

Robinsion, W. A., 1988: Analysis of LIMS data by potential inversion. *J. Atmos. Sci.*, **45**, 2319–2342.

Stoelinga, M. T., 1996: A potential-vorticity based study of the role of diabatic heating and friction in a numerically simulated baroclinic cyclone. *Mon. Wea. Rev.*, **124**, 849–874.

Tao Shiyan, Zhang Xiaoling, and Zhang Shunli, 2004: Rainstorms in Meiyu front. Chapter 3, *A Study on the Disasters of Heavy Rainfalls over the Yangtze River Basin in the Mei-Yu Period.* China Meteorological Press, Beijing, 39–116. (in Chinese)

Xing Qian, and Zheng Weizhong, 1999: A mesoscale cyclone numerical simulation and analysis of a heavy rain process in the Changjiang-Huaihe River basin. *Scientia Meteorologica Sinica*, **19**, 242–250. (in Chinese)

Zhao Bingke, 2006: A study on the mechanism of cyclogenesis over the Yangtze River and Huaihe River valleys in summer. Ph. D. dissertation, Institute of Atmospheric Physics, Chinese Academy of Sciences, 133pp. (in Chinese)

Zhao Bingke, Yao Xiuping, and Wu Guoxiong, 2005: The structure and activity characteristics of the western Pacific subtropical anticyclone and its dynamical mechanism during the Mei-Yu period over the Huaihe basin in 2003. *Chinese J. Atmos. Sci.*, **29**, 771–779. (in Chinese)

Zhao Sixiong, Tao Zuyu, Sun Jianhua, and Bei Naifang, 2004: *Study of Weather Systems during Heavy Rainfalls on Meiyu Front.* Chapter 2, *Study on the Mechanism of Formation and Development of Heavy Rainfalls on the Meiyu Front in the Yangtze River.* China, Meteorological Press, Beijing, 21–65. (in Chinese)